

Response Enhancement of Self-Powered Visible-Blind UV Photodetectors by Nanostructured Heterointerface Engineering

Tao Zhu, Jun Su, J Alvarez, Grégory Lefèvre, Frédéric Labat, Ilaria Ciofini, Thierry Pauporte

▶ **To cite this version:**

Tao Zhu, Jun Su, J Alvarez, Grégory Lefèvre, Frédéric Labat, et al.. Response Enhancement of Self-Powered Visible-Blind UV Photodetectors by Nanostructured Heterointerface Engineering. Advanced Functional Materials, 2019, 29, pp.1903981. 10.1002/adfm.201903981 . hal-02236553

HAL Id: hal-02236553
https://hal.science/hal-02236553

Submitted on 12 Nov 2020

HAL is a multi-disciplinary open access archive for the deposit and dissemination of scientific research documents, whether they are published or not. The documents may come from teaching and research institutions in France or abroad, or from public or private research centers.

L'archive ouverte pluridisciplinaire **HAL**, est destinée au dépôt et à la diffusion de documents scientifiques de niveau recherche, publiés ou non, émanant des établissements d'enseignement et de recherche français ou étrangers, des laboratoires publics ou privés.

Please cite this paper as

Tao Zhu, Jun Su, José Alvarez, Grégory Lefèvre, Frédéric Labat, Ilaria Ciofini, Thierry Pauporté

Response Enhancement of Self-Powered Visible-Blind UV Photodetectors by Nanostructured Heterointerface Engineering
Adv. Funct. Mater., 29 (2019) 1903981.
DOI: 10.1002/adfm.201903981

Mr. T. Zhu, Dr. G. Lefèvre, Prof. Th. Pauporté
Chimie ParisTech, PSL Research University, CNRS, Institut de Recherche de Chimie Paris (IRCP), 11 rue P. et M. Curie, F-75005 Paris, France.
E-mail: thierry.pauporte@chimie-paristech.fr

Mr. J. Su, Dr. F. Labat, Prof. I. Ciofini
Chimie ParisTech, PSL Research University, CNRS, Institute of Chemistry for Life and Health Sciences (i-CLeHS), 11 rue P. et M. Curie, F-75005 Paris, France.

Dr. J. Alvarez
Laboratoire de Génie électrique et électronique de Paris (GeePs), UMR 8507 CNRS CentraleSupelec, Univ. Paris-Sud Universite Paris-Saclay, Sorbonne Universite, 11 rue Joliot-Curie, F-91192 Gif-sur-Yvette, France.

Keywords: photodetector, self-powered, visible-blind, interface modifier, modeling

The development of efficient photodetectors (PDs) for ultra-violet (UV) light is of great importance for many applications. In the present paper, we propose a novel approach for boosting the performances of self-powered PDs. Visible-blind UV-A PDs have been built by combining a mesoporous TiO_2 layer with a Spiro-OMeTAD layer. The nanostructured heterointerface has been engineered by inserting a self-assembled layer of organic modifiers. By choosing the 4-nitrobenzoic acid (NBA), the responsivity has been boosted by 70% compared to the pristine devices. It achieved 64 mA/W at 0 V bias, 380 nm and 1 $mW.cm^{-2}$. The PD displayed a very high sensitivity (> 10^4), a fast response time (< 3ms), a high stability and repeatability. 4-chlorobenzoic acid, 4-methoxy benzoic acid, 4-nitro benzoic acid and β-alanine surface modifier have been studied by a combined experimental and theoretical approach. Their dipole moment has been calculated. Their presence induces a step in the

vacuum energy and the formed dipole field dramatically affects the charge transfer and then the photocurrent/photoresponse of the device. The higher responsivity of the NBA-modified PD has been thus explained by the better and faster electron charge transfer towards the electrical contact on TiO_2.

1. Introduction

The efficient photodetection of ultra-violet (UV) light has drawn considerable attention owing to it great importance in various and often strategic fields.[1-12] Systems have been designed for applications in environmental and biological analysis or monitoring, flame detection, military applications, geology detection, space communication, chemical and pharmaceutical analyses and industrial quality control.[2-4] Si-based technologies are well-established for these applications. However, due to the narrow (1.12 eV) and indirect bandgap of crystallized Si semiconductor (SC), the UV-enhanced Si technology requires the use of costly high-pass filters and phosphors to stop low energy photons. The use of thin films is preferable to save material. Moreover, wide-bandgap SCs allow the direct UV detection and visible wavelength irradiation rejection without any additional device components. Among the potential candidates, oxides such as ZnO or TiO_2 are of utmost interest due to their possible preparation as thin or nanostructured films from solutions. They have the advantage to be insensitive to the visible light and, therefore, they allow a visible-blind detection without any additional filters or phosphors.[8,9] Oxide active two-dimensional (2D) layers have been studied in UV-photodetectors (PDs) in a large extent.[13] Oxide one-dimensional (1D) structures, especially nanowire (NW) arrays, also present an interesting sensitivity to light for the application.[10-12] Furthermore, oxide NWs have allowed the miniaturization of the PD systems with the successful fabrication, in the recent years, of single-nanowire PDs, an approach which is also interesting to realize flexible self-powered PDs.[4,6]

Conventional UV-Photodetectors need to be driven by an external power source, such as a battery, to present suitable responsivities. It generates undesirable extra-cost, requires maintenance and generates environmental concerns. Alternatively, self-powered systems, which harvest their energy from the environment, are sustainable, maintenance-free and self-contained. In most cases, they are driven by a built-in electric field.[4] There are three main strategies described in the literature to achieve self-powering: (i) p-n homojunction PDs, (ii) p-n heterojunction PDs and (iii) Schottky-junction based PDs. The preparation of high quality fully inorganic p-n heterojunction requires high temperature and/or vacuum and is costly.[14,15]

On the other hand, oxide wide bandgap semiconductor layers and nanostructured films can be prepared easily from solutions and at low cost for n-type doping.[4,11,16] However, the synthesis of the p-type counterparts remains difficult and getting highly transparent p-type oxide is still challenging. Therefore, alternative solutions, easy to implement, must be proposed. Moreover, technological solutions to boost their detection properties are desirable.

There are many organic compounds that can be used for hole transport and which are p-doped.[17,18] Organic p-type SCs can be essentially divided into two subclasses: molecular and polymeric compounds.[19,20] The former is advantageous in terms of processability, thermomechanical stability, and higher intrinsic hole mobility. The latter is beneficial in terms of synthetic reproducibility, well-defined molecular weight and structure. Combining an inorganic n-type oxide with an organic p-type material in hybrid heterostructures in type II heterojunctions is a promising approach for the UV-A (320 nm to 400 nm) detection. In the first attempts, polymers were combined with oxides. Li *et al*. proposed a nanostructured near-UV photodetector based on ZnO nanorod/polyfluorene hybrid devices, which demonstrated a high responsivity of 0.18 A/W at 300 nm at -2 V. [21] Also p-type polyaniline (PANI) layers have been combined with various oxide n-type SC for the fabrication of UV-PDs such as p-polyaniline (*p*-PANI)/*n*-TiO_2,[22] *p*-PANI/*n*-MgZnO,[23] *n*-ZnO/*p*-PANI/*n*-ZnO.[24] However, the reported responsivities were poor with a best value at 3.6 mA/W at 320 nm.[4,22] The use of molecular p-type SC has been poorly explored. While polymers with a conjugated chain present a rather good intrinsic conductivity, the molecular p-type SCs exhibit a low conductivity and require additives to be implemented in optoelectronic devices.[19,20] Some authors have investigated 2,2',7,7'-tetrakis(N,N-di-p-meth-methoxyphenylamine)- 9,9'-spirobifluorene (Spiro-MeOTAD) for the p-type layer in UV-PDs. This compound has a rather high T_g (above 125 °C) which is promising to achieve high device thermal stability. [25-27] It has been combined with various nanostructured wide bandgap oxide layers. Xie et al.[28] prepared UV-PDs based on Spiro-OMeTAD and TiO_2 nanorod arrays while Game et al. [29] investigated the combination of this molecular compound with ZnO NRs. Bai et al.[27] used a mesoporous TiO_2 layer as the n-type nanostructure. Molecular p-type SCs, especially Spiro-OMeTAD, allow a high pore filling of mesoporous nanostructured films. However, the maximum device responsivities were reported at 17 mA/W,[28] 10 mA/W,[29] and 18 mA/W.[27]

The literature survey shows the need of boosting the responsivity of self-powered hybrid UV-PDs. In the present paper we propose a novel approach for this purpose. UV-A PDs have been built by combining a dense and mesoporous TiO_2 bilayer with a Spiro-OMeTAD layer. These devices have been shown to be visible-blind. The interface between the two layers has

been engineered by inserting a self-assembled layer of organic modifiers. In the fabrication process, the use of additives in the Spiro-OMeTAD has been avoided to prevent any interfacial change by these compounds and to improve the device stability. These interfacial modifiers presented a carboxylic acid group for their anchoring at the oxide surface and a second para-functional group. It has resulted in a dipole moment which introduces a step of the vacuum level energy. Depending on the orientation of this dipole moment, an electric field is generated which assists or prevents the charge transfer at the heterojunction. By accurately choosing the modifier (*ad-hoc* functional group), we have been able to increase by 70% the responsivity of the hybrid UV-A PDs. The adsorption of the modifiers on the TiO_2 surface has been modeled by periodic Density Functional Theory (DFT) calculations. The normal component of the dipole moments to the exposed TiO_2 surface has been calculated and the trends obtained have been found in agreement with work function measurements. These combined studies have allowed confirming the dramatic effect of the interfacial energetics on the charge separation and device performances. Moreover, we have shown that these devices present an excellent reproducibility, an excellent spectral selectivity and a fast dynamic response.

2. Results and discussion

The device structure is presented in Figure 1a. The FTO/glass substrate was covered by a thin, dense and pinhole-free TiO_2 layer prepared by spray pyrolysis.[30] Its role was to avoid the direct contact between the Spiro-OMeTAD and the FTO. Then a TiO_2 mesoporous layer (*mp*-TiO_2) composed of nanoparticles with an average 30 nm diameter was added. This layer was treated with various acids in order to produce an interlayer as shown in Figure 1b. The investigated acids were parasubstituted benzoic acid derivatives with various dipole direction and strength: 4-chlorobenzoic acid (CBA), 4-methoxy benzoic acid (MBA) and 4-nitro benzoic acid (NBA). Additionally, β-alanine (β-ALA), an amino-acid, was also investigated. Our theoretical study (reported below) shows that their carboxylic acid function is dissociated on the surface, that they interact with TiO_2 by their $–COO^-$ group, attached in a bidendate bridging mode. They form self-assembled monolayers (SAMs). The device was completed by a Spiro-OMeTAD layer and a gold back contact. No additive was used with Spiro-OMeTAD in order to avoid any other interaction with TiO_2 and interfacial modification.[20]

The devices were characterized by measuring their *J-V* curve under 365 nm UV-light. The initial curves are shown in Figure S1 (Supporting Information). A photovoltaic effect was found but the recorded curves were S-shaped, whether the interface was acid-modified or not. The devices did not work correctly. An undoped Spiro-OMeTAD layer has a low conductivity (estimated at about 3.10^{-7} $S.cm^{-1}$ in our previous work [20]). Charge extraction is then difficult and we suggest that charge accumulation occurs at the interface that plays on the recombination process.[31]

After storage of the devices in air, a dramatic change in the *J-V* response was found. The S-shape disappeared, the J_{sc} increased while the V_{oc} were unchanged (Figure S1b, Supporting Information). The unencapsulated devices were then highly stable and showed no electrical characteristics change within several months of storage under ambient conditions. The maturation is explained by the oxidation of the Spiro-OMeTAD layer. Oxidation by O_2 in air occured, produced the p-type doping of the molecular SC and then its dramatic increase in conductivity. According to the literature,[20] the oxidation reaction can be written:

$$\text{Spiro-OMeTAD} + O_2 \rightarrow \text{Spiro-OMeTAD}^{\bullet+}O_2^{\bullet-} \qquad (1)$$

Figure 2a and S1b (Supporting Information) show that the current density at 0 V bias varies in a large extent with the modifier. The order is NBA> CBA> Blank> β-ALA> MBA. Remarkably, the photocurrent was increased by 70% with the NBA treatment compared to the blank and it was 10% increased by the CBA treatment. On the other hand, this parameter was reduced for the other acids, especially with MBA. In Figure S1b (Supporting Information), an interesting information is that the open circuit potential varied inversely compared to the J_{sc} for the blank and para-substituted benzoic acids modifiers. The order is β-ALA> MBA> Blank> CBA> NBA for the matured PDs (Table S1, Supporting Information). This series follows the order of the dark current (Figure S1c, Supporting Information): the lower the dark current, the higher the V_{oc}. For the benzoic acid derivatives, the dark J-V curves reported in the present work are in good agreement with Ref.[32].

Figure 2b and Figure S2a (Supporting Information) detail the response of the PD to UV-light for the NBA-modified and the blank devices, respectively. The dark current curve is typical of a p-n junction diode behavior with a clearly rectifying *J-V* characteristic. The rectification ratio (*RR*), i.e. the dark current ratio measured at +1 V and -1 V, is high at about 900 for the blank and 400 for the NBA-PD. Under UV-Light, the current density continuously increased with the light irradiance. One of the advantages of operating the PD at 0 V bias or at low bias is the very high dynamic range. The sensitivities (J_{light}/J_{dark}) at 0 V for the various devices are gathered in Table S2 (Supporting Information). Very high and remarkable values are found, above 10^4 for all the PDs, except the MBA-modified PD which exhibits slightly lower values.

The absorbance spectrum of the prepared devices (without the Au backcontact) is shown in Figure 3a as a dashed line. The absorbance is rather flat and very low over most of the visible/NIR wavelength region. An absorption edge appears below 410 nm. It is due to light absorption in the Spiro-OMeTAD which bandgap, at about 3.0 eV (Figure S2b, Supporting Information), is slightly lower than the anatase TiO_2 one.[33] In the same figure, the quantum efficiency (EQE) curves for the various PDs are also plotted. The EQE spectra follow the absorbance spectrum. They present a maximum at about 380 nm. The EQE maximum is measured for the NBA PD at 21%. Figure 3b shows the responsivity (*R*) spectra of the various PDs. This parameter is defined as :

$$R = \frac{EQE(\%)\lambda q}{hc} \qquad (2)$$

with λ the radiation wavelength, *q* the elemental charge, *h* the Planck constant and *c* the light velocity. The maximum of the responsivity is achieved with the NBA device at 64 mA/W. It is much higher than the values reported in the literature for the hybrid organic/inorganic UV-PDs.[22-24, 27-29] The hybrid devices exhibit more than a two-orders of magnitude difference while illuminated in the UV and in the visible light range. The rejection ratio, defined as the

ratio of *R* between 380 nm and 520 nm, is gathered in Table S1 (Supporting Information) for the various devices. A value of 159 is found for the NBA PD.

Three other parameters of great importance for any PDs are the response time, the repeatability and the stability as they often determine the suitability of a device for a specific application. The photocurrent time response was measured at 0 V bias under 365 nm light source on/off sudden switching irradiation. Figure 4a shows that the photoresponse of the NBA-modified device under alternate on/off cycles is highly repeatable and stable. A similar behavior is found with the other devices in Figure 4b. Figure 4a and 4b display abrupt rises and decays in the photocurrent response. We have calculated the rise and decay times for the various PDs. The former is defined by the time in which the photocurrent rises from 10% to 90% of its maximum value. The latter is the time to drop from 90% to 10% of the photocurrent maximum value. The devices had remarkable fast response times, measured at less than 3 ms (the measurement step of the current recording system) for the rise time. The decay time was measured at 3 ms or less for all the PDs except for the β-ALA one which was measured at 6.5 ms. The long-term stability of the devices is also an important parameter for the practical application. Figure S1d (Supporting Information) shows a degradation of the performances of the unencapsulated blank device stored under ambient conditions for several months. On the other hand, the NBA PD exhibits a remarkable stability. The J_{sc} is almost unchanged after 156 days of storage and the SAM plays a key role in the stabilization.

The above results show that the PD performances can be significantly altered by adsorbing acids to modify the *mp*-TiO_2/Spiro-OMeTAD interface and that high performances are reached by using NBA as a molecular interface modifier. The adsorption and the chemical nature of the adsorber are key parameters for tuning the devices responsivity. The adsorption of the acids has been further studied by the FTIR technique. Figure 5 compares the FTIR absorbance spectra of the four acids dissolved in an organic solvent (black curves) and adsorbed onto TiO_2 particles

(red curves). An experimental procedure was specifically designed to get reliable spectra in the latter case which is detailed in the Experimental Section.

For the benzoic acid derivatives, we observe a band at 1680-1723 cm^{-1} (twinned in the case of NBA and CBA) which are assigned to a C=O stretching vibration.[34-39] This mode is shifted in the case of β-ALA and found at 1633 cm^{-1}. These bands disappeared in all cases after the attachment onto the TiO_2 surface. The bands observed at 1533 cm^{-1} (NBA), 1595 cm^{-1} (CBA) and 1604/1595/1515 cm^{-1} (MBA) remained after the binding of the benzoic acid derivatives and are assigned to C=C stretching modes. For β-ALA, bands are observed at 1572 cm^{-1} and 1502 cm^{-1} which correspond to antisymmetric and symmetric bending modes, respectively.[40,41] For all the isolated acids, a band is found at 1261-1265 cm^{-1} which is assigned to the COO symmetric stretching mode (ν_s), while the bands at 1347 cm^{-1} (NBA) /1401 cm^{-1} (CBA)/ 1428 cm^{-1} (MBA)/ 1399 cm^{-1} (β-ALA) are assigned to the antisymmetric stretching mode (ν_{as}) of −COO. The assignment has been confirmed by DFT calculations (refer to Table S3 in the Supporting Information). After adsorption, these modes were significantly shifted at higher wavenumbers (frequency) and found at 1415 cm^{-1} (NBA)/ 1413 cm^{-1} (CBA)/ 1410 cm^{-1} (MBA)/ 1409 cm^{-1} (β-ALA) for ν_s and 1566 cm^{-1} (NBA)/ 1593 cm^{-1} (CBA)/ 1591 cm^{-1} (MBA)/ 1580 cm^{-1} (β-ALA) for ν_{as}.

To gain a deeper insight into the effect of the modifiers on the interface energetic, electronic and vibrational properties, the adsorption of the various acids on the (101) anatase TiO_2 surface (the most stable one [42]) has been modeled by DFT. Our first objectives were to determine the binding mode, the adsorption energy and the structural features of the molecules adsorbed onto the surface. The most favorable adsorption mode has been found to be the bridging bidendate one. Computed adsorption energies are gathered in Table S3 (Supporting Information). Data in the literature support a dissociative adsorption mechanism [32] and a bidentate adsorption mode for carboxylic acids bound on anatase surface, consistent with the acidity of this group.[43,44] The dissociative process is written:

$$-COOH \rightarrow -COO^- + H^+ \qquad (3)$$

The O-H bond is broken and the H^+ atom is connected to an O atom on the anatase surface (Figure S3 and Table S4, Supporting Information). In the bidendate bridging mode, each oxygen atom in the −COO functional group is bound to a different Ti atom of the surface, with very similar O-Ti distances. Figure S3 (Supporting Information) presents the optimized DFT structure of CBA adsorbed on TiO_2 both (a) without and (b) with an explicit methanol solvent molecule. A large tilting of the benzene ring compared to the vertical position is observed. This tilting is found for all the benzoic acid derivatives and for β-ALA (Figure 6). The tilt angle versus the surface normal (θ_a) is reduced and the molecules are straightened when an explicit solvent molecule (here methanol which is the solvent used experimentally for the acid treatment of the surface) is considered. For instance, the angle changed from 42° to 30° in the case of CBA (Figure S3, Supporting Information). θ_a for the various acids are gathered in Table 1. The tilting is more relevant for the benzoic acids compared to β-ALA due to the π-interaction between H^+ atom on the surface and the ring.

Then, the harmonic vibrational frequencies were computed and compared with available FTIR spectra. The calculated -COO ν_{as} and ν_s wavenumbers are given in Table S3 (Supporting Information). Δ_1 is the wavenumber difference between the theoretical calculations and the experimental results. A generally good agreement is obtained between the computed and the experimental data. In particular, in most cases, Δ_1 is lower than 50 cm^{-1}, and a shift at higher wavenumbers is obtained after the molecule binding to the TiO_2 surface. The computed wavenumber difference between the antisymmetric and the symmetric stretching modes (Δ_2) is, as expected, the same for all the isolated benzoic acid derivatives (180 cm^{-1}) and slightly lower in the case of isolated β-ALA. On the other hand, for the adsorbed compounds, Δ_2 varies as a function of the acid considered. When adsorption occurs, the environment for COO- bond changes, its symmetric and antisymmetric stretchings are affected and Δ_2 value decreases. This change may also indicate the dissociation process of carboxylic acid. Furthermore, the

experimental and the computed values are close as reported in Table S3 (Supporting Information), thus validating the model developed. In particular, this confirms that a bridging bidentate binding mode is obtained for all ligands adsorbed on TiO_2.

Due to the polarization of these molecules, their adsorption induces the presence of a dipole moment at the TiO_2 surface.[45] The dipole component normal to the surface ($\mu_\perp$) introduces a step in the local vacuum level due to the electric field across this layer. The work function and the band edge of the TiO_2 surface are changed by $q\Delta V$. ΔV is expressed by the Poisson's equation:

$$\Delta V = \frac{N_s \mu \cos \theta_a}{\varepsilon_r \varepsilon_0} \qquad (4)$$

with N_s the surface dipole density, μ the dipole moment, θ_a the tilt angle of the dipole versus the surface normal, ε_r the dielectric constant and ε_0 the permittivity of free space.

$\mu_\perp$ values, calculated by DFT for the various acids, are gathered in Table 1. The order is NBA> CBA> β-ALA> MBA. We note that $\mu_\perp$ of MBA is negative (dipole moment pointing toward TiO_2 in the chemistry notation). In the same table, we also report the values calculated for the free molecules. After adsorption, the magnitude of all the dipole moments decreased due to two phenomena: a charge transfer to the TiO_2 surface combined to the tilting of the molecules on the surface. More precisely, from computed Mulliken atomic charges, while a charge transfer to the TiO_2 surface of about 0.26 $|e^-|$ is computed for CBA, NBA and MBA, β-ALA shows a lower charge transfer of about 0.21 $|e^-|$.

The present results show the strong influence of adsorption on the μ value and that the modeling of the adsorption of the ligands on the TiO_2 surface is required to properly discuss dipole moment effects.

The change in the local vacuum level has been then quantified by Kelvin probe measuring the work function of the bare TiO_2 layer and of the modified TiO_2 layers. The results are shown

in Figure 7. For the blank and the benzoic acids, a linear relationship is found which is in agreement with Equation (4). A special behavior is found for β-ALA, the point being outside the straight line. The dark current behavior in Figure S1c and the work function measurements suggest that its dipole moment should be negative.

From the above results, the enhancement of the PD photoresponse in the UV by the interfacial modification of the p-n heterojunction can be explained. The presence of the dipoles at the interface introduces an additional electric field. When the dipole field is pointing outward titania, the vacuum level is shifted upward and the work function is increased. When electron-hole pairs are photogenerated in the Spiro-OMeTAD layer, the electrons are drifted toward the TiO_2 layer, the charge separation and transfer are facilitated and the measured photocurrent is enhanced. On the contrary, for the adsorbed molecules with a dipole moment pointing toward the oxide, the vacuum energy level is shifted downward, the work function is reduced. An interfacial electric field is present that reduces the electron charge transfer toward TiO_2 and then, the generated photocurrent in the PD.

These phenomena are schematically presented in Figure 8. Figure 8 also shows the effect of the modifier on the V_{oc}. The V_{oc} is limited by the $E_c(TiO_2)$-E_{HOMO}(Spiro-OMeTAD) gap. The presence of a dipole layer changes this gap: it is reduced for a dipole with a positive $\mu_\perp$ (Figure 8a) and increased for a dipole with a negative $\mu_\perp$ (Figure 8c). Therefore, in the former case, the V_{oc} will be reduced while this parameter will be increased in the latter case. This phenomenon is clearly observed for the benzoic acid derivatives series (see Figure S1, Supporting Information).

3. Conclusion

In conclusion, we have designed and fabricated a solid-state nanostructured UV-A photodetector based on the TiO_2/Spiro-OMeTAD p-n heterojunction. No additive was used in

the Spiro-OMeTAD layer. The doping was achieved by the oxidation of the layer in air. This approach has permitted the reliable study of the effect of interfacial modifiers on the PD response. The prepared diode had a rectifying ratio of 900. We have shown that the UV-PD could be used in a self-powered mode. We have carefully investigated the effect of interfacial modifiers on the PD functioning and performances and we have concluded in their strong effect. The NBA modifier has permitted to boost the responsivity of the device by 70% compared to the pristine p-n junction. The responsivity was measured at 64 mA/W at 0 V and 380 nm. The PDs were visible-blind due to the large bandgap (3 eV) of the Spiro-OMeTAD and the rejection ratio between the UV-A and the visible light was measured higher than two orders of magnitude. The device sensitivity (J_{light}/J_{dark}) at 0 V was remarkably high, above 104. Moreover, we have found that their UV-light switching on/off was highly repeatable and that their photoresponse was stable. The response time was measured very fast, below 3 ms. The NBA devices were also shown highly stable.

The acid modifier adsorption has been then thoroughly investigated by a combined experimental and theoretical approach. They are adsorbed at the TiO_2 surface by their carboxylate group in a bridging bidendate mode. The theoretical FTIR spectra have been found in general good agreement with the experimental ones and clearly show the binding of the molecular dipole onto the oxide surface. The surface normal component of the dipole moment of the compounds has been calculated. Their presence induces a step in the vacuum energy and the formed dipole field dramatically affects the charge transfer and the photocurrent of the device. The higher responsivity of the NBA-modified PD is then explained by the better and faster electron charge transfer towards the electrical contact on TiO_2.

4. Experimental Section

Preparation of the TiO_2 layer: Fluorine-doped SnO_2 (FTO) substrates (TEC 7 from Pilkington) were etched by zinc powder and 10 % HCl solution and then cleaned with soap and water. The

preliminary cleaned substrates were immersed in a concentrated 2.2 M NaOH ethanol/water (10:1 v/v %) for 20 min and then cleaned with deionized water under ultrasonics for 15 min. The substrates were subsequently heated at 500 °C for 15 min.

The TiO_2 blocking layer was prepared by an aerosol spray pyrolysis technique as described in a previous work.[30] The obtained TiO_2 layer was dense, pinhole-free and 30-35 nm thick.[30] The TiO_2 paste for the preparation of the mesoporous layer was prepared in advance and stirred for at least 12 h. The TiO_2 NR30-D paste (from Greatcell) was diluted in ethanol with a 1:7 w/w ratio.[46] 45 µL of the prepared TiO_2 paste was dropped and spin-coated on the compact TiO_2 layer, then quickly transferred to an hotplate at 70 °C and dried for 5-10 min. Finally, the formed mesoporous layer was heated at 500 °C under an air flux for 30 min, cooled down to 200 °C and removed from the hotplate. The *mp*-TiO_2 layer morphology is displayed in Figure S4 (Supporting Information).

TiO_2 surface modification: Four different acids were investigated for the mesoporous layer surface modification: 4-chlorobenzoic acid (CBA), 4-methoxy benzoic acid (MBA); 4-nitro benzoic acid (NBA) and β-alanine (β-ALA). Their molecular structures are displayed in Figure 1b and Table S4 (Supporting Information). 1 mg of these compounds was dissolved in 1mL methanol. The mesoporous layers were transferred into a dry glovebox. The SAMs were deposited on TiO_2 layer by spin-coating. 65 µL of the acid solutions were dropped on the mesoporous layer, reacted 30s before starting the spin-coater at a speed of 3000 rpm for 10 s. The samples were subsequently placed on a hotplate at 100 °C for 10 min. The same procedure was used again with pure methanol (washing with pure methanol, spin-coating and annealing at 100 °C for 10 min) for removing the reactant excess.

The work function of the bare TiO_2 and acid-modified TiO_2 layers was investigated using a Kelvin probe system from KP Technology (ASKP200250) equipped with a 2 mm diameter steel probe. The stability of the probe work function was evaluated on a gold reference sample provided by KP Technology which work function was taken at 4800 meV vs vacuum.

The adsorption of the acid molecules was investigated by an attenuated total reflection (ATR-IR) technique inspired from our previous study.[47] The infrared spectra of molecules isolated and bound to TiO_2 nanoparticles were measured in a dry air-purged compartment of a ThermoScientific Nicolet 6700 spectrometer equipped with a mercury cadmium telluride (MCT) detector. A 1 mg/mL TiO_2 nanoparticle aqueous solution was prepared. A droplet of this solution was deposited on the system diamond crystal and dried under argon blowing. This process was repeated twice. The crystal was capped with a flow cell. First a reference spectrum consisting of TiO_2 in contact with ethanol was recorded. Afterwards, starting the circulation system, the 10^{-3} M solution of acid was flowed past on the TiO_2 covered diamond crystal and the spectrum was recorded until no evolution of the signal was observed and then until the equilibrium state was reached (after 20-30 min). The baseline of these spectra was the ethanol/TiO_2 spectrum. The spectra of the isolated acids were recorded by depositing directly a concentrated solution (10^{-1} M) of benzoic acid derivatives on the naked diamond crystal. A lower concentration, corresponding to its solubility limit, $<10^{-2}$ M, was used in the case of β-ALA. We have checked that the results with ethanol solvent were the same as those with methanol, the solvent used for surface modification. The concentrations of the solutions employed in this experiment are gathered in Table S5. (Supporting Information)

Device preparation and characterizations: A solution was prepared by dissolving 72 mg of Spiro-OMeTAD (Borun New Material Technology) in 1 mL of chlorobenzene. 40 μL of this solution was spin-coated on the bare and modified TiO_2 layers at 4000 rpm for 20 s. We chose not to dope the layer with oxidizing agents because these additives can be detrimental for the stability of the device and can modify the interface. The samples with Spiro-OMeTAD layer were transferred into a nitrogen filled glovebox for one night. The devices were completed by evaporating a 80 nm thick gold contact in a vacuum chamber.

The heterojunction absorbance was measured with a Cary 5000 UV-Vis-NIR spectrophotometer. The *J-V* curves were recorded by a Keithley 2410 digital sourcemeter at a

50 mV/s scan rate. The p-n junctions were measured in the dark and under illumination with a 365 nm UV LED lamp at controlled irradiance (between 0.55 mW/cm^2 and 200 mW/cm^2). The irradiance was calibrated using a coherent fieldmaxII powermeter. The active surface area was about 0.26 cm^2. No mask was used and the devices were illuminated through the glass substrate. The external quantum efficiency (EQE) spectra were measured using an Oriel QUANTX-300 system. The light beam was chopped at 77 Hz. The monochromatic illumination was calibrated by a NIST-calibrated Si photodiode. The presented results are from devices that were stored more than one month under ambient conditions.

DFT investigation of acid adsorption: All calculations were carried out with the ab initio CRYSTAL17 code,[48] which is based on a linear combination of atom-centered Gaussian orbitals and solves self-consistently Hartree-Fock and Kohn-Sham equations.

The (101) surface of the anatase phase of TiO_2 was considered for the adsorption of the ligands since this surface is well-known to be highly stable.[49-51] A two-dimensional periodic slab with 4-Ti layers was cut out from the TiO_2 anatase bulk system ($I4_1/amd$ space group) with the following PBE0-D3 optimized cell parameters: 3.7578 Å (a), 9.7039 Å (c). The slab obtained here is used as a starting point for the adsorption, and a rectangular (2x1) supercell was considered in order to avoid artificial interaction between adsorbates from one cell to the other due to the 2D periodicity of the model. The *a* and *b* lattice parameters for this supercell slab model are 7.4906 Å and 5.5442 Å, respectively, corresponding to a surface coverage of one ligand molecule per 3.9 nm^2. Sampling of the irreducible Brillouin zone was done with 7 k points along the a* and b* directions of these systems, corresponding to a total number of 25 k points. Numerical DFT integration was performed considering 75 radial points and 974 angular points, ensuring an error on the integrated electron density lower than 10^{-5} |e-| per unit cell. The Coulomb and exchange series were truncated with threshold values of 10^{-7}, 10^{-7}, 10^{-7}, 10^{-7}, and 10^{-18}.

Organic ligands were described using all electron basis sets with (621/21/1), (7311/311/1), (8411/411/1), (511/1) and (86311/6311) for C, N, O, H and Cl atoms, respectively. Durand and Barthelat large core pseudopotentials with (1/1/41) and (31/31) contractions were used for Ti and O atoms of the TiO_2 substrate, respectively.[52,53]

Exchange and correlation energies were described using the global hybrid PBE0 functional,[54] with 25% of HF exchange. Additional D3 dispersion corrections were also included.[55]

To simulate the experimental environment, the solvent, methanol, was added to the models, considering a molecular binding mode to the TiO_2 surface. As described in the result section, this allows limiting the tilting of the different ligands adsorbed on the surface.

For adsorption energies (E_{ads}), total adsorption energies of ligand and methanol ($E_{ads\text{-}total}$) were first computed, as the difference between the total energies ($E_{adsorbate\text{-}surface}$) of the combined adsorbate/substrate system and the sum of the relaxed energies of a TiO_2 surface with a H^+ ($E_{surface+H}$) and a negatively charged adsorbate molecule in the gas phase ($E_{ligand\text{-}}$), and a methanol molecule in the gas phase (E_{CH3OH}) as:

$$E_{ads\text{-}total} = E_{adsorbate\text{-}surface} - (E_{surface+H} + E_{ligand\text{-}} + E_{CH3OH})$$

The adsorption energy of methanol $E_{ads\text{-}methanol}$ was calculated with the following formula:

$$E_{ads\text{-}methanol} = E_{CH3OH\text{-}surface} - (E_{surface} + E_{CH3OH})$$

with $E_{CH3OH\text{-}surface}$ corresponding to the difference of the total energy of the CH_3OH/TiO_2 system and the sum of the relaxed energies of a bare TiO_2 surface and the CH_3OH molecule. Finally, the adsorption energies of the ligands ($E_{ads\text{-}ligand\text{-}}$) were computed as the difference between $E_{ads\text{-}total}$ and $E_{ads\text{-}methanol}$:

$$E_{ads\text{-}ligand\text{-}} = E_{ads\text{-}total} - E_{ads\text{-}methanol}$$

A negative value of $E_{ads\text{-}ligand}$ corresponds a thermodynamically favored adsorption process.

During geometry optimization, only atomic positions were allowed to relax, while lattice parameters were constrained to those of the supercell mentioned above. Numerical harmonic

frequency calculations were performed at the Γ-point on the optimized structures in order to compute the IR spectra of the adsorbed molecules. To limit computational cost, only the first TiO_2 layer and the adsorbed ligand and methanol molecule were included in the Hessian construction. Test calculations including more TiO_2 layers showed negligible differences with values discussed here.

Supporting Information
Supporting Information is available from the Wiley Online Library or from the author.

Acknowledgements
T.Z. and S.J acknowledge the CSC-Paristech and CSC program for Ph.D scholarship. Bruno Viana is acknowledged for his help in UV-photodetection measurements and equipment loan.

Received: ((will be filled in by the editorial staff))
Revised: ((will be filled in by the editorial staff))
Published online: ((will be filled in by the editorial staff))

References

[1] M. Razeghi, A. Rogalski, *J. Appl. Phys.* **1996**, 79, 7433.

[2] L. Sang, M. Liao, M. Sumiya, *Sensors* **2013**, 13, 10482.

[3] Z. Alaie, S. M. Nejad, M. H. Yousefi, *Mater. Sci. Semicond. Process.* **2015**, 29, 16.

[4] L. Su, W. Yang, J. Cai, H. Chen, X. Fang, *Small* **2017**, 13, 1701687.

[5] V. Postica, M. Hoppe, J. Gröttrup, P. Hayes, V. Röbisch, D. Smazna, R. Adelung, B. Viana, P. Aschehoug, T. Pauporté, O. Lupan, *Solid State Sci.* **2017**, 71, 75.

[6] O. Lupan, V. Postica, R. Adelung, N. Ababii, L. Chow, B. Viana, T. Pauporté, *Proc. SPIE*, **2017**, 101051Y. doi:10.1117/12.2249841.

[7] K. Liu, M. Sakurai, M. Aono, *Sensors* **2010**, 10, 8604.

[8] H. Kind, H. Yan, B. Messer, M. Law, P. Yang, *Adv. Mater.* **2002**, 14, 158.

[9] Y. Zou, Y. Zhang, Y. Hu, H. Gu, *Sensors* **2018**, 18, 2072.

[10] H. Zhang, A. V. Babichev, G. Jacopin, P. Lavenus, F. H. Julien, A. Yu. Egorov, Th. Pauporté, M. Tchernycheva, *J. Appl. Phys.* **2013**, 114, 234505.

[11] O. Lupan, S. Koussi-Daoud, B. Viana, T. Pauporté, *RSC Advances* **2016**, 6, 68254.

[12] T. Pauporté, O. Lupan, V. Postica, M. Hoppe, L. Chow, R. Adelung, *Physica Status Solidi (a)* **2018**, 215, 1700824. DOI: 10.1002/pssa.201700824.

[13] H. Shen, C. Shan, B. Li, B. Xuan, D. Shen, *Appl. Phys. Lett.* **2013**, 103, 232112.

[14] C. -L. Hsu, Y. -D. Gao, Y. -S Chen, T. -J. Hsueh, *ACS Appl. Mater. Interfaces* **2014**, 6, 4277.

[15] B. Zhao, F. Wang, H. Chen, L. Zheng, L. Su, D. Zhao, X. Fang, *Adv. Funct. Mater.* **2017**, 27, 1700264.

[16] O. Game, U. Singh, T. Kumari, A. Banpurkarc, S. Ogale, *Nanoscale* **2014**, 6, 503.

[17] I. E. Jacobs, A. J. Moulé, *Adv. Mater.* **2017**, 29, 1703063.

[18] J. Burschka, A. Dualeh, F. Kessler, E. Baranoff, N.-L. Cevey-Ha, C. Yi, M. K. Nazeeruddin, M. Grätzel, *J. Am. Chem. Soc.* **2011**, 133, 18042.

[19] M. Ulfa, T. Zhu, F. Goubard, T. Pauporté, *J. Mater. Chem. A* **2018**, 6, 13350.

[20] M. Ulfa, T. Pauporté, T. T. Bui, F. Goubard, *J. Phys. Chem. C* **2018**, 122, 11651.

[21] Y. Li, C. Chen, W. Yen, W. Su, C. Ku, J. Wu, *Appl. Phys. Lett.* **2008**, *92*, 233301.

[22] L. Zheng, P. Yu, K. Hu, F. Teng, H. Chen, X. S. Fang, *ACS Appl. Mater. Interfaces* **2016**, 8, 33924.

[23] H. Chen, P. Yu, Z. Zhang, F. Teng, L. Zheng, K. Hu, X. S. Fang, *Small* **2016**, 12, 5809.

[24] S. Yang, J. Gong, Y. Deng, *J. Mater. Chem.* **2012**, 22, 13899.

[25] T. Leijtens, I-K. Ding, T. Giovenzana, J. T. Bloking, M. D. McGehee, A. Sellinger, *ACS Nano* **2012**, 6, 1455.

[26] T. -T. Bui, M. Ulfa, F. Maschietto, A. Ottochian, M. -P. Nghiem, I. Ciofini, F. Goubard, T. Pauporté, *Org. Electron.* **2018**, 60, 22.

[27] H. Bai, T. Shen, J. Tian, *J. Mater. Chem. C* **2017**, 5, 10543.

[28] Y. Xie, L. Wei, Q. Li, G. Wei, D. Wang, Y. Chen, J. Jiao, S. Yan, G. Liu, L. Mei, *Appl. Phys lett.* **2013**, 103, 261109.

[29] O. Game, U. Singh, T. Kumari, A. Banpurkarc, S. Ogale, *Nanoscale*, **2014**, 6, 503.

[30] P. Wang, Z. Shao, M. Ulfa, T. Pauporté, *J. Phys. Chem. C* **2017**, 121, 9131.

[31] A. Sundqvist, O. J. Sandberg, M. Nyman, J. H. Smatt, R. Osterbacka, *Adv. Energy. Mater.* **2016**, 6, 1502265.

[32] J. Kruger, U. Bach, M. Gratzel, *Adv. Mater.* **1999**, 12, 447.

[33] C. Magne, F. Dufour, F. Labat, G. Lancel, O. Durupthy, S. Cassaignon, T. Pauporté, *J. Photochem. Photobiol. A* **2012**, 232, 22.

[34] N. Sundaraganesan, B. Anand, C. Meganathan, B. Joshua, *Spectrochimica Acta Part A: Molecular and Biomolecular Spectroscopy* **2008**, 69, 871.

[35] X. Luo, J. Shen, X. Zhao, Z. Wang, B. Wu, L. Li, X. Zhou, *Inorg. Chim. Acta* **2016**, 446, 169.

[36] S. Badilescu, P. Ashrit, V. Truong, *Appl. Phys. Lett.* **1988**, 52, 1551.

[37] S. Hyouk, H. Chang, H. Kim, K. Kim, *Appl. Spectrosc.* **1998**, 52, 1047.

[38] S. Shao, F. Liu, G. Fang, B. Zhang, Z. Xie, L. Wang, *Org. Electron.* **2011**, 12, 641.

[39] M. A. Palafox, M. Gil, J. Nunez, *Appl. Spectrosc.* **1994**, 48.1, 27.

[40] M. Mohamed Ali Jinnah, M. Umadevi, V. Ramakrishnan, *J. Raman Spectrosc.* **2004**, 35.11, 956.

[41] M. T. S. Rosado, M. L. R.S. Duarte, R. Fausto, *J. Mol. Struct.* **1997**, 410, 343.

[42] F. Labat, P. Baranek, C. Adamo, *J. Chem. Theory Comput.* **2008**, 4, 341.

[43] A. G. Thomas, J. J. Mark, W. Michael, R. Hanna, S. Karen, A. Johan, L. Anna, M. Natalia, *Langmuir* **2014**, 30, 12306.

[44] F. Labat, C. Adamo, *J. Phys. Chem. C* **2007**, 111, 15034.

[45] C. Goh, S. R. Scully, M. D. McGehee, *J. Appl. Phys.* **2007**, 101, 114503.

[46] M. Ulfa, P. Wang, Z. Shao, B. Viana, T. Pauporté, *Proc. SPIE* **2018**, 105332R. doi: 10.1117/12.2294941.

[47] T. Le Bahers, T. Pauporté, F. Labat, G. Lefèvre, I. Ciofini, *Langmuir* **2011**, 27, 3442.

[48] R. Dovesi, V. Saunders, C. Roetti, R. Orlando, C. Zicovich-Wilson, F. Pascale, B. Civalleri, K. Doll, N. Harrison, I. Bush, *Crystal* **2006**, 06.

[49] A. Barnard, P. Zapol, *Phys. Rev. B* **2004**, 70, 235403.

[50] A. Barnard, P. Zapol, L. Curtiss, *Surf. Sci.* **2005**, 582, 173.

[51] C. Arrouvel, M. Digne, M. Breysse, H. Toulhoat, P. Raybaud, *J. Catal.* **2004**, 222, 152.

[52] J. Berthelat, P. Durand, *Gazzetta Chimica Italiana* **1978**, 108, 225.

[53] J. Barthelat, P. Durand, A. Serafini, *Molecular Physics* **1977**, 33, 159.

[54] C. Adamo, V. Barone, *J. Chem. Phys.* **1999**, 110, 6158.

[55] S. Grimme, G. Semiempirical, *J. Comput. Chem.* **2006**, 27, 1787.

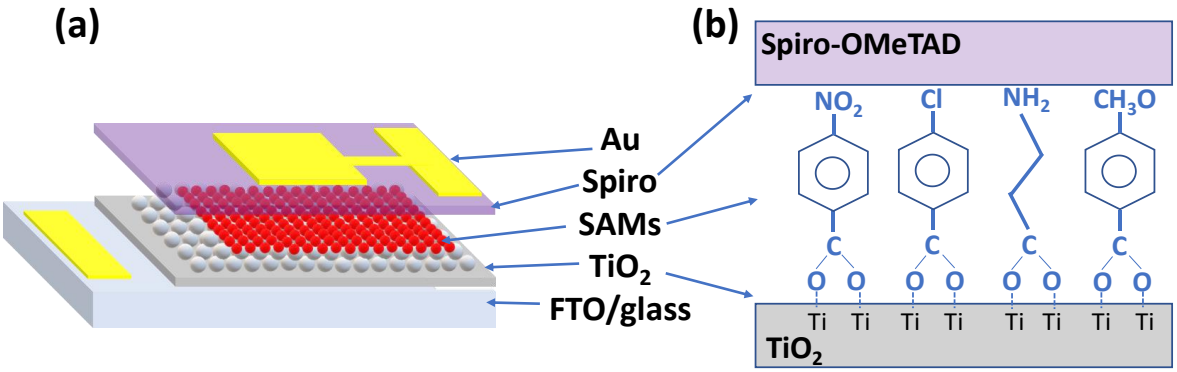
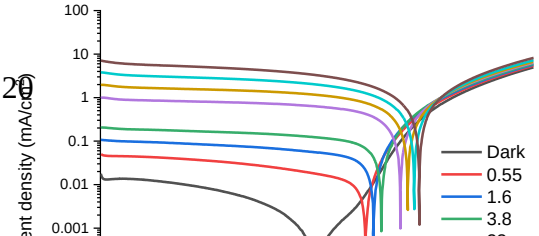


Figure 1. (a) Photodetector exploded schematic view. (b) Schematic of the acids self-assembled interlayer between TiO_2 and Spiro-OMeTAD. From left to right: 4-nitrobenzoate (NBA); 4-chlorobenzoate (CBA); beta-alanine (β-ALA) and 4-methoxybenzoate (MBA).



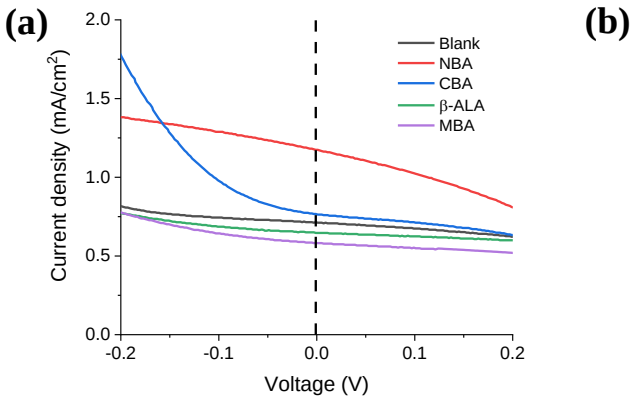


Figure 2. (a) Effect of the molecular modifier on the current recorded under an irradiance of 47 mW/cm^2 (λ=365 nm). (b) Current density-voltage (*J*-*V*) curves in the dark and for increasing light irradiance of the matured NBA-modified PD (λ=365 nm).

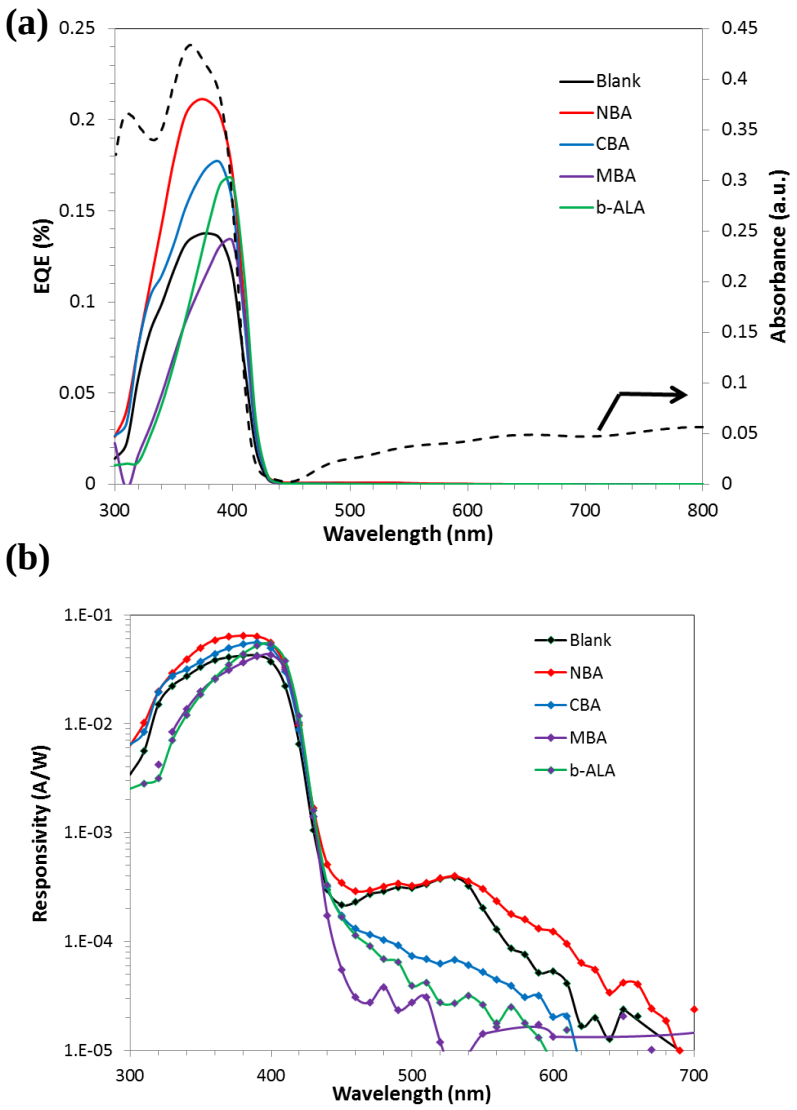


Figure 3. (a) Device absorbance spectrum and EQE curves of the various PDs. (b) Responsivity spectra of the various PDs.

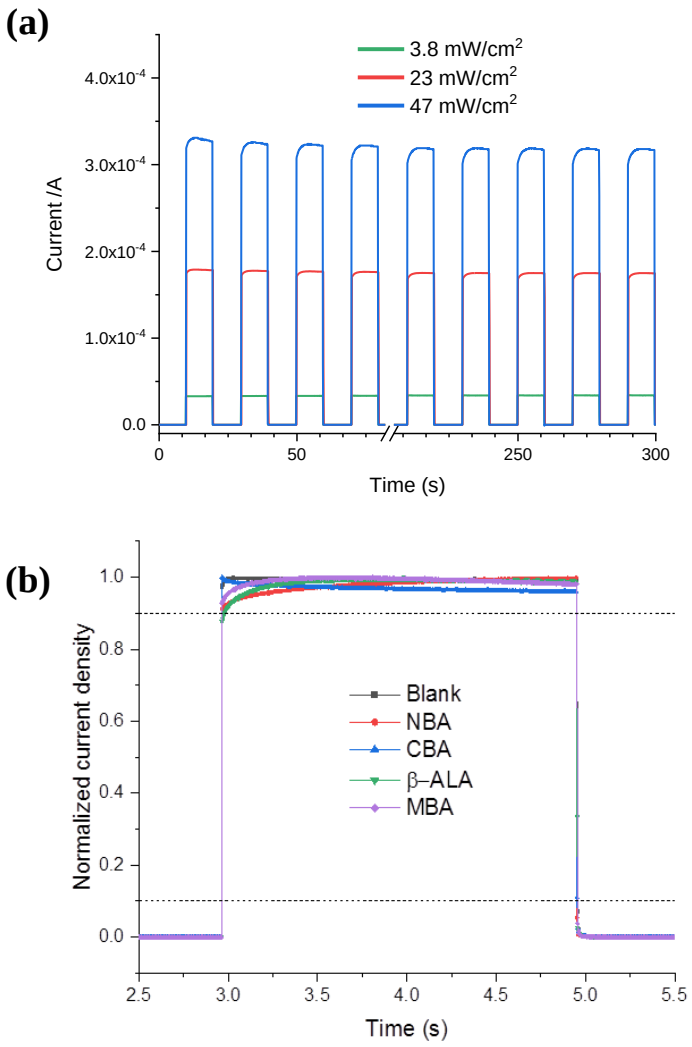


Figure 4. (a) Time-response of the NBA-PD under alternate switch on/ switch off UV-Light at various irradiances. (b) Effect of surface modifier on the normalized time response of the PDs. (λ=365 nm)

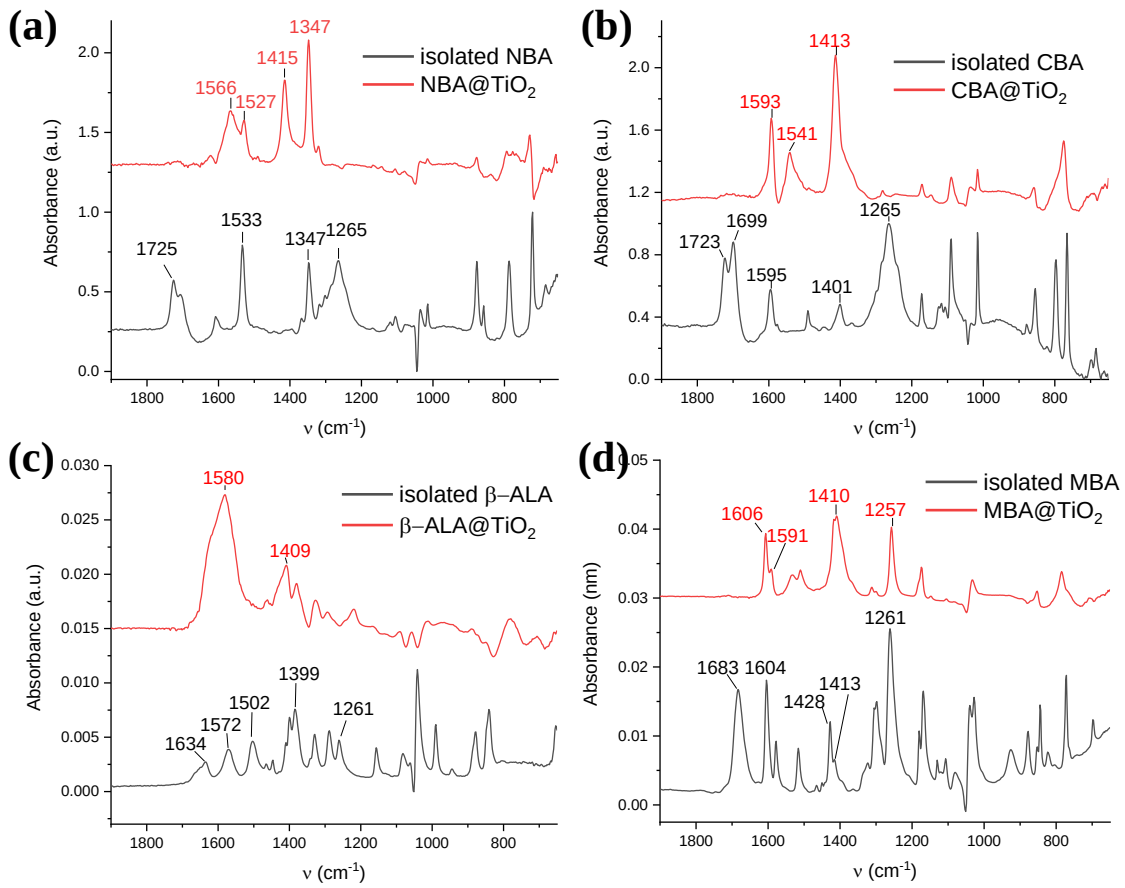


Figure 5. FTIR spectra of the modifiers dissolved in ethanol (black) and adsorbed on TiO_2 nanoparticles (red). (a) NBA, (b) CBA, (c) β-ALA and (d) MBA.

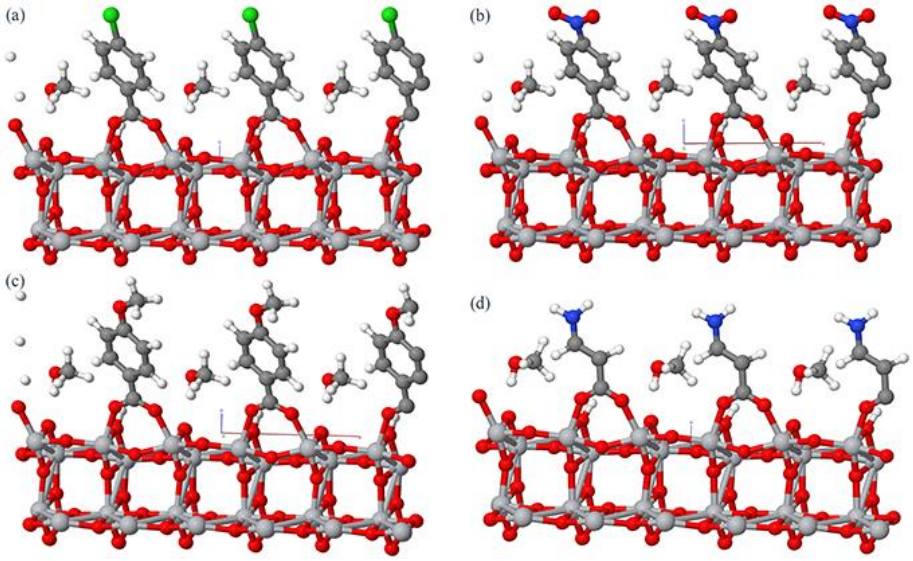


Figure 6. Optimized structure of the 4 acids adsorbed onto anatase (101) surface in the presence of methanol. The carbon, titanium, oxygen, chloride and nitrogen atoms are represented by grey, silver, white, red, green and blue balls, respectively. (a) CBA, (b) NBA, (c) MBA and (d) β-ALA.

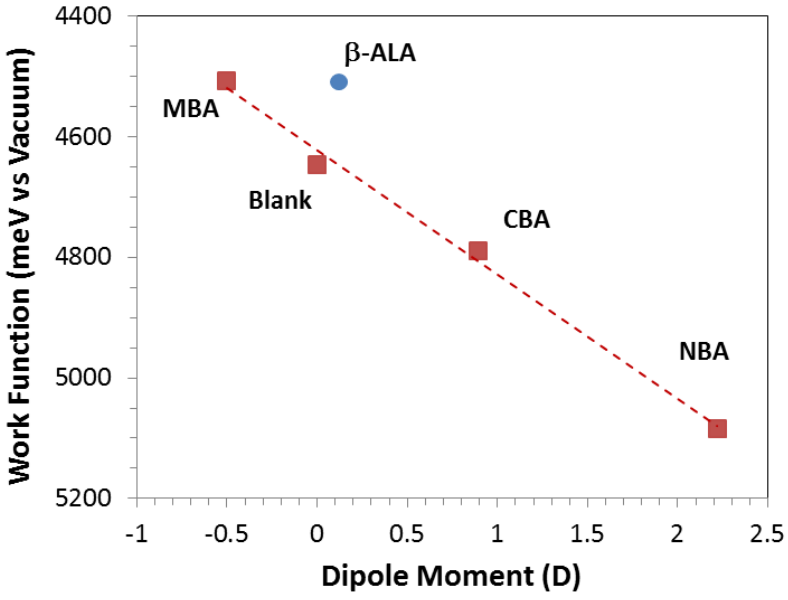


Figure 7. Work function versus the calculated dipole moment ($\mu_{\perp}$) of the molecules adsorbed onto TiO_2.

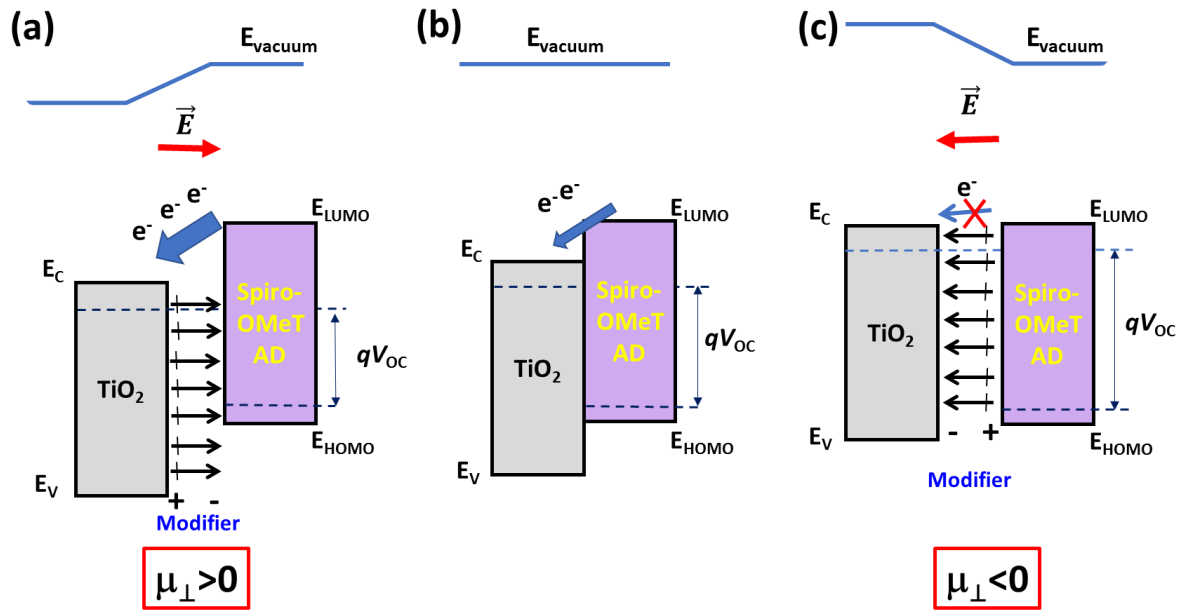


Figure 8. Effect of the interfacial dipole modifiers on the energetics of the TiO_2/Spiro-OMeTAD p-n heterojunction. (a) Dipole inducing a $\mu_\perp > 0$ at the interface; (b) pristine interface and (c) dipole inducing a $\mu_\perp < 0$ at the interface.

Table 1. Calculated structural tilt angle (θ_a), adsorption energy and normal component of the dipole moment with respect to the TiO_2 surface of the acids adsorbed onto TiO_2 ($\mu_\perp$). Corresponding total dipole moment values for the isolated molecules are reported in brackets.

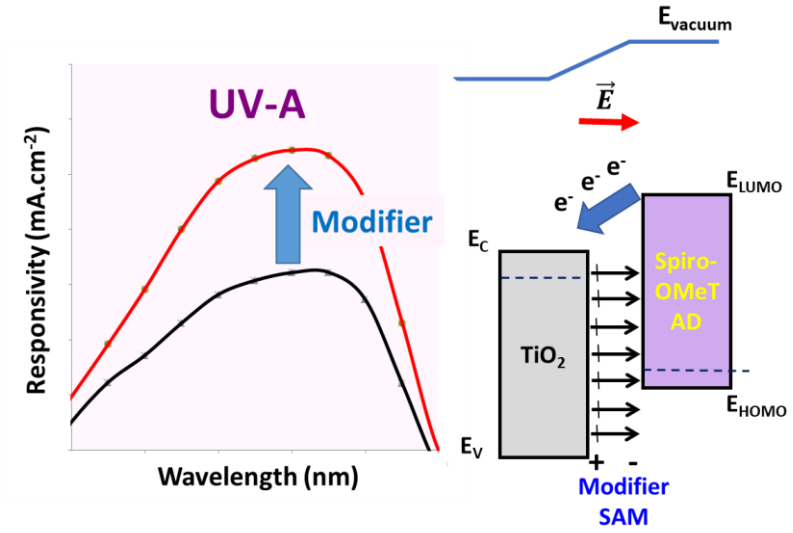
	NBA	CBA	β-ALA	MBA
θ_a (°)	31.6	30.3	13.4	30.6
Adsorption Energy (kcal/mol)	-11.3	-20.7	-20.2	-30.6
$\mu_\perp$(D)	2.22 (3.72)	0.89 (1.55)	0.12 (2.79)	-0.5 (-2.57)

Keyword: photodetector, self-powered, visible-blind, interface modifier, SAMs, modeling

Tao Zhu,a Jun Su, José Alvarez, Grégory. Lefèvre, Frédéric Labat, Ilaria Ciofini, Thierry Pauporté*

Response Enhancement of Self-Powered Visible-Blind UV Photodetectors by Nanostructured Heterointerface Engineering

ToC figure



Short summary

We propose a novel approach for boosting the performances of self-powered photodetectors. Visible-blind devices have been built by combining a mesoporous TiO_2 layer with a Spiro-OMeTAD layer. The nanostructured heterointerface has been engineered by inserting a self-assembled monolayer of 4-nitrobenzoic acid. The introduced molecular dipole field dramatically favors the charge transfer and the photocurrent of the device.

Supporting Information

Response Enhancement of Self-Powered Visible-Blind UV Photodetectors by Nanostructured Heterointerface Engineering

*Tao Zhu, Jun Su, José Alvarez, Grégory. Lefèvre, Frédéric Labat, Ilaria Ciofini, Thierry Pauporté**

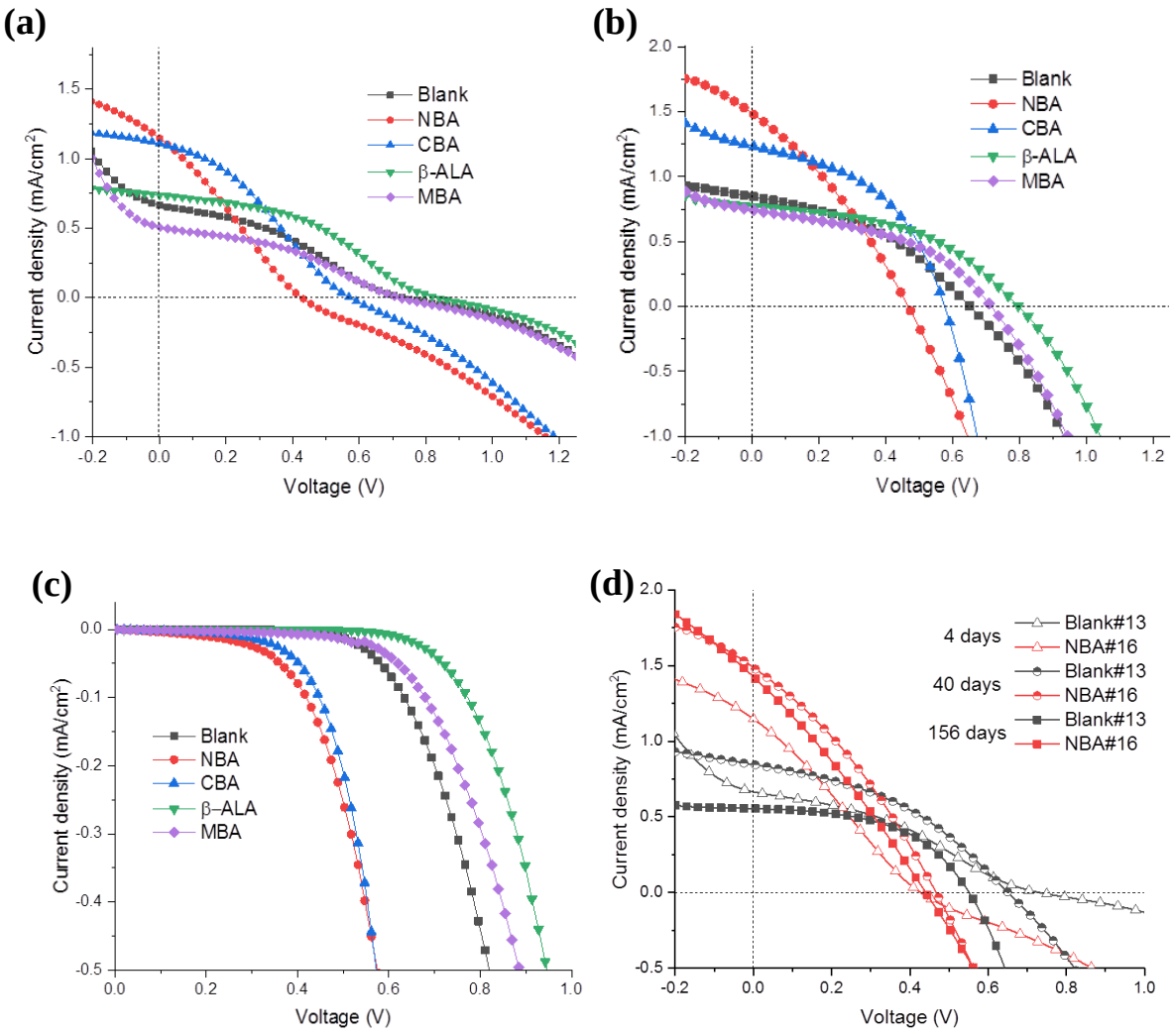


Figure S1. Current density-Voltage (*J-V*) curves under UV light (λ=365 nm, 40 mW.cm^{-2}). (a) Initial and (b) after 40 days of storage under ambient conditions. (c) Dark current after one month of storage. (d) *J-V* curves of unencapsulated blank (black traces) and NBA (red traces) PDs after 4, 40 and 156 days of storage under ambient conditions.

Table S1. Effect of acid treatment on the open circuit voltage (λ=365 nm, 40 mW.cm^{-2}) and rejection ratio[a] of the matured PDs

	Blank	NBA	CBA	MBA	β–ALA
V_{oc} (V)	0.651	0.466	0.575	0.714	0.796
Rejection Ratio[a]	113	159	865	3000	1600

[a]Ratio between the responsivity at 380 nm and at 520 nm.

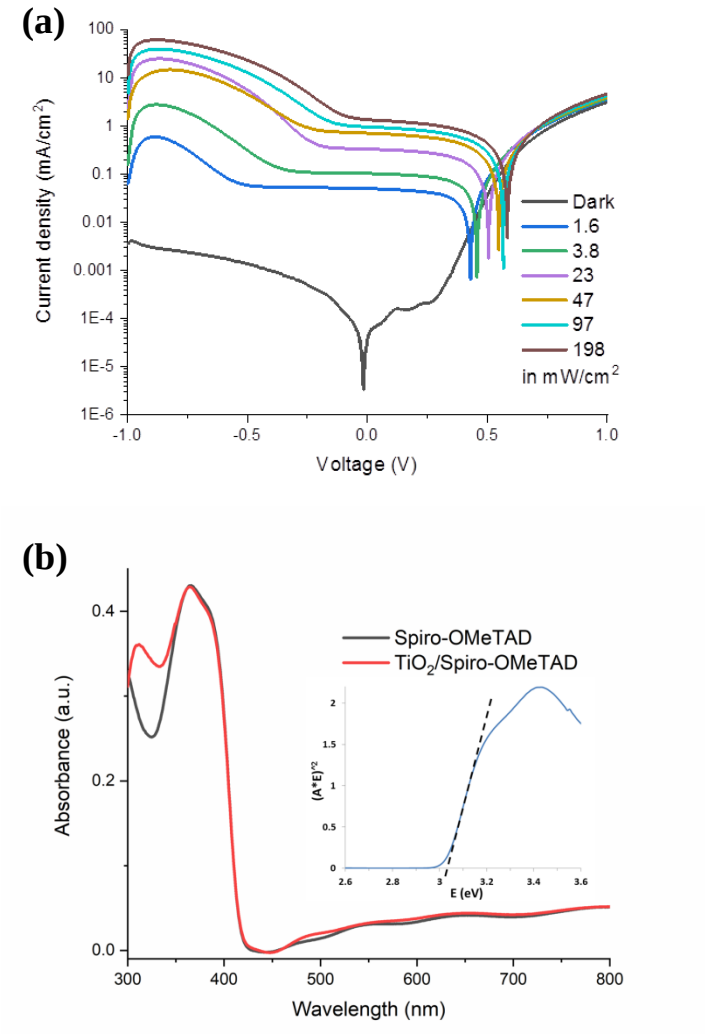


Figure S2. (a) *J-V* curves of the Blank (unmodified) PD in the dark and under various irradiances. (b) Absorbance curves of the Spiro-OMeTAD and TiO_2/Spiro-OMeTAD layers.

Table S2. Sensitivity (J_{light}/J_{dark}) of the PDs at 0V bias (λ=365 nm).

Sample	23 mW/cm^2	47 mW/cm^2
NBA	$1.2\ 10^4$	$2.3\ 10^4$
CBA	$8.9\ 10^3$	$1.5\ 10^4$
Blank	$9.2\ 10^3$	$2.0\ 10^4$
ALA	$1.6\ 10^4$	$2.4\ 10^4$
MBA	$5.1\ 10^3$	$7.9\ 10^3$

Table S3. Selected computed and experimental IR wavenumbers of isolated acids and acids on anatase surface. Δ_1 is the difference between the experimental and calculated data, and Δ_2 is the difference between the wavenumber of symmetric (ν_s) and antisymmetric (ν_{as}) stretching of -COO bonds. All data in cm^{-1}.

		Isolated			Adsorbed@TiO_2		
		Calc.	Exp.	Δ_1	Calc.	Exp.	Δ_1
CBA	ν_s	1215	1265	50	1472	1413	-59
	ν_{as}	1395	1401	6	1590	1593	3
	Δ_2	180	136		118	180	
NBA	ν_s	1215	1265	50	1473	1415	-58
	ν_{as}	1395	1347	-48	1598	1566	-32
	Δ_2	180	82		125	151	
MBA	ν_s	1219	1261	42	1467	1410	-57
	ν_{as}	1399	1428	29	1585	1591	6
	Δ_2	180	167		118	181	
β-ALA	ν_s	1218	1261	43	1497	1409	-88
	ν_{as}	1392	1399	7	1585	1580	-5
	Δ_2	174	138		88	171	

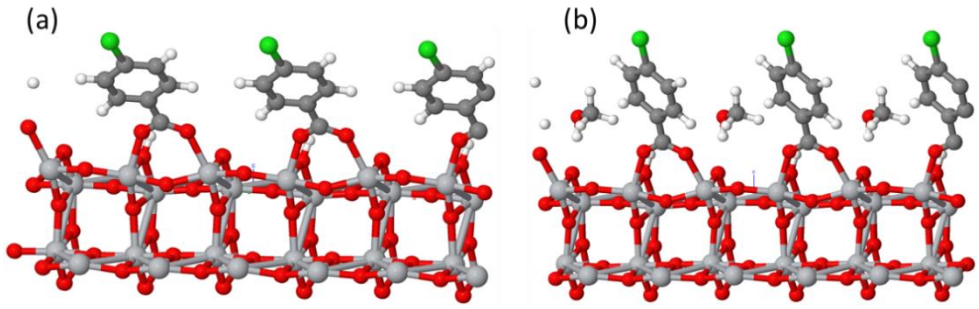
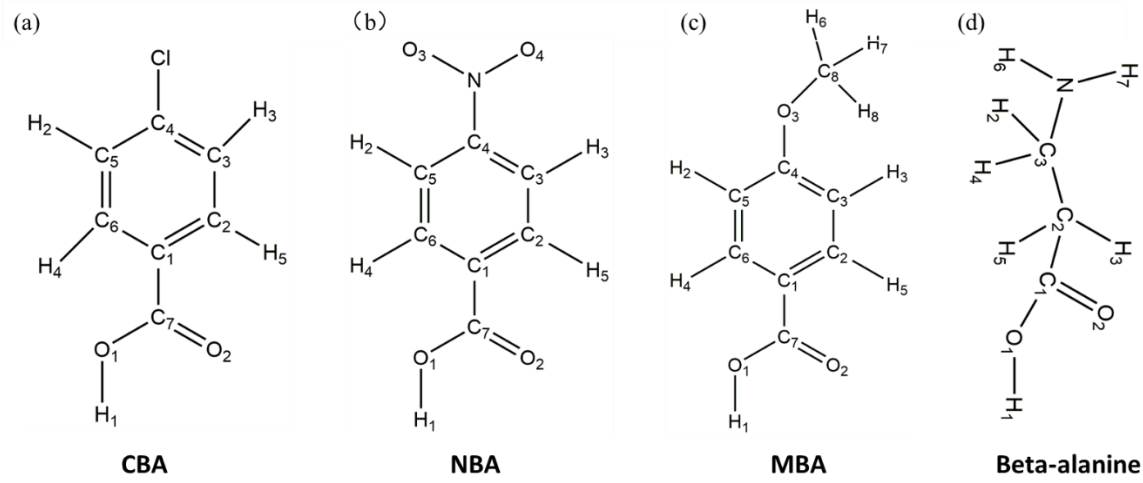


Figure S3. Optimized structure of CBA molecules adsorbed on anatase TiO_2 (101) surface without (a) and with (b) methanol solvent. The carbon, titanium, oxygen, chloride and nitrogen atoms are represented by grey, silver, white, red, green and blue balls, respectively.

Table S4. Molecular structure and atom labelling of (a) CBA, (b) NBA, (c) MBA and (d) β-ALA. Selected geometrical parameters (Angles in deg; Distances in Å) for isolated and adsorbed molecular systems and corresponding adsorption energies (in kcal/mol) and tilt angle to the surface normal (θ_a).



Distance(Å)	CBA	CBA@TiO_2	Distance(Å)	NBA	NBA@TiO_2
dO_1C_7/dO_2C_7	1.35/1.21	1.26/1.27	dO_1C_7/dO_2C_7	1.35/1.21	1.26/1.27
dC_1C_7/dC_4Cl	1.48/1.79	1.48/1.79	dC_1C_7/dC_4N	1.49/1.47	1.49/1.48
dH_2C_5/dH_3C_3	1.09/1.09	1.09/1.09	dH_2C_5/dH_3C_3	1.09/1.08	1.08/1.08
dH_4C_6/dH_5C_2	1.09/1.09	1.08/1.09	dH_4C_6/dH_5C_2	1.09/1.09	1.08/1.09
dO_1Ti/dO_2Ti	-	2.15/2.06	dO_3N/dO_4N	1.22/1.22	1.22/1.22
			dO_1Ti/dO_2Ti	-	2.16/2.05
Θ_a		30.3°	Θ_a		31.6°
$E_{ads\text{-}ligand\text{-}}$		-20.73	$E_{ads\text{-}ligand\text{-}}$		-11.33

Distance(Å)	MBA	MBA@TiO_2		Beta-Alanine	Beta-Alanine@TiO_2
dO_1C_7/dO_2C_7	1.35/1.21	1.27/1.27	dO_1C_1/dO_2C_1	1.35/1.21	1.26/1.27
dC_1C_7/dC_4O	1.47/1.36	1.48/1.35	dC_1C_2/dC_2C_3	1.51/1.54	1.51/1.52
dH_2C_5/dH_3C_3	1.09/1.09	1.09/1.08	dC_3N_1	1.46	1.46
dH_4C_6/dH_5C_2	1.09/1.09	1.08/1.09	dH_2C_2/dH_3C_2	1.10/1.09	1.10/1.10
$dOC_8/dH_{6\text{-}8}C_8$	1.41/1.10	1.35/1.10	dC_3H_4/dC_3H_5	1.10/1.10	1.10/1.09
dO_1Ti/dO_2Ti	-	2.16/2.04	dNH_6/dNH_7	1.02/1.01	1.02/1.01
			dO_1Ti/dO_2Ti	-	2.13/2.08
Θ_a		31.6°	Θ_a		13.4°
$E_{ads\text{-}ligand\text{-}}$		-30.62	$E_{ads\text{-}ligand\text{-}}$		-20.20

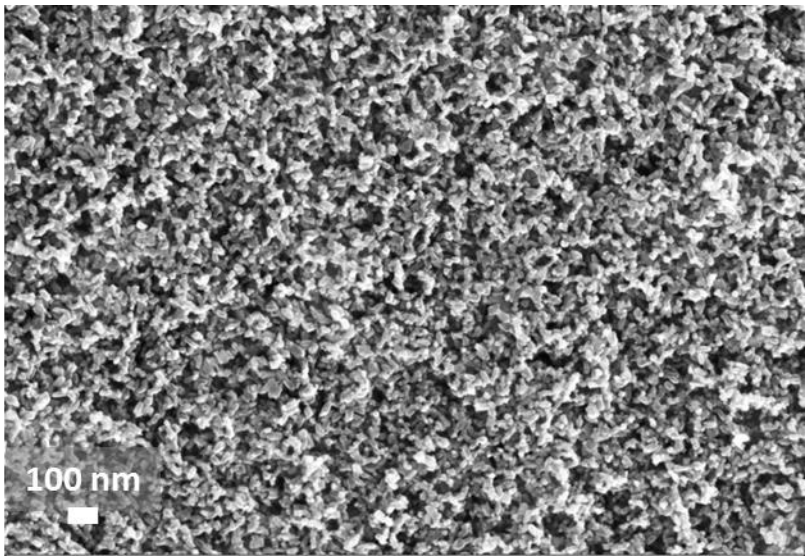


Figure S4. SEM top view of the *mp*-TiO_2 mesoporous layer which is modified by the treatment with various acids.

Table S5. Solution concentration used for the FTIR study of free acids and acids adsorbed onto TiO_2 nanoparticles.

Volume	TiO_2	CBA	MBA	NBA	β-Alanine	solvent
10mL		10^{-1} M	10^{-1} M	10^{-1} M	$<10^{-2}$ M	ethanol
50mL		10^{-3} M	10^{-3} M	10^{-3} M	10^{-3} M	
5mL	1 mg/mL	10^{-1} M				methanol